Supplementary Materials for

Temporal patterning of apical progenitors and their daughter neurons in the developing neocortex

L. Telley*, G. Agirman, J. Prados, N. Amberg, S. Fièvre, P. Oberst, G. Bartolini, I. Vitali, C. Cadilhac, S. Hippenmeyer, L. Nguyen, A. Dayer, D. Jabaudon*

*Corresponding author. Email: ludovic.telley@unil.ch (L.T.); denis.jabaudon@unige.ch (D.J.)

This PDF file includes:

Materials and Methods
Figs. S1 to S10
Tables S1 and S2
References
Descriptions of data S1 to S8

Other supplementary material for this manuscript includes:

Data S1 to S8 (Excel format)

Materials and Methods

Mice

All experiments were approved by the Geneva Cantonal Veterinary Authorities, Switzerland and the Austrian Federal Ministry of Science and Research in accordance with the Austrian and EU animal laws. CD1 WT mice were purchased from Charles River Laboratories and the embryonic day (E) 0 (three-hour time-mated females) or E0.5 (overnight-mated females) was established as the time of detection of the vaginal plug. In addition, the *Eed-flox* allele (*49*), *Emx1*-Cre (*50*) were used. MADM-*GT* and -*TG* cassettes (Chr. 7) were present in these lines (*51*) but this feature was not used here; the genetic background for these lines was mixed C57/Bl6, CD1. Both female and male animals were analyzed in this study.

Genotyping of transgenic mice

Biopsies were collected and DNA extraction and PCR amplification were performed using the Phire Animal Tissue Direct PCR Kit (Thermo Scientific, #F-140WH) and following manufacturer's instructions. The following primers (5'-3') were used: Eed for - GGG ACG TGC TGA CAT TTT CT; Eed rev - CTT GGG TGG TTT GGC TAA GA; Cre for - GTC CAA TTT ACT GAC CGT ACA CC; Cre rev - GTT ATT CGG ATC ATC AGC TAC ACC. Cre^{+}/Eed$^{+/+}$ animals were used as WT, and Cre^{+}/Eed$^{fl/fl}$ as Eed cKO.

In utero FlashTag injection

FlashTag (FT) injections were performed between E12 and E15, as previously described (*13*). Briefly, pregnant females were anaesthetized with isoflurane, treated with Temgesic (Reckitt Benckiser, Switzerland) and the uterine horn was exposed following an abdominal incision. Half a microliter of 10 mM of a carboxyfluorescein succinimidyl ester (*i.e.* FlashTag, CellTrace™ CFSE, Life Technologies, #C34554) was injected into the lateral cerebral ventricle of the embryos. The abdominal wall was then closed and the embryos were let to develop until collection.

Immunofluorescence

Tissue processing: Embryonic brains were dissected in a phosphate-buffered saline (PBS) solution, fixed in 4% paraformaldehyde (PFA) overnight at 4°C then cryoprotected in PBS-sucrose

30% overnight at 4°C before embedding in OCT and freezing on dry ice. Postnatal mice were perfused with 4% PFA, brains were dissected and post-fixed in 4% PFA overnight at 4°C then stored in PBS. Coronal brain sections were performed using either a cryostat (embryonic brains; 14 µm) or a vibrating microtome (postnatal brains; 70 µm).

Immunofluorescence on brain sections: Brain sections were incubated 30min at 85°C in citrate buffer solution and washed 3 times in PBS prior to a 1-hour incubation in blocking solution (10% horse serum - 0,5% Triton X-100 diluted in PBS) at room temperature. Slides were then incubated overnight at 4°C with primary antibodies. Next, slides were washed 3 times in PBS and incubated 2 hours at room temperature with respective secondary antibodies (1:500). When applied, EdU was revealed following the manufacturer's instructions using Click-it chemistry (Invitrogen). Finally, slides were mounted with Fluoromount (Sigma). In Fig. 6A, the H3K27me3 image intensity range was normalized to the brightest juxtaventricular VZ cells at each embryonic age.

Immunofluorescence on in vitro culture: Cells were fixed in 4% PFA for 15 min, treated with 0.25% Triton X-100 for 20 min and blocked in 0.5% BSA, 0.25% Triton X-100 for 1 hour at room temperature. Primary antibody incubations were performed overnight at 4° C, and secondary antibody incubations were performed 1 hour at room temperature. Coverslips were mounted on slides using Fluoromount (Sigma).

Antibodies: rat anti-BrdU (1:200, Abcam, #AB6326), goat anti-BRN2 (1:500; Thermo Scientific, #PA5-1904), rat anti-CTIP2 (1:500, Abcam, #AB18465), rabbit anti-FITC (1:500, Abcam, #AB19491), rabbit anti-H3K27me3 (1:500, Millipore, 07-449 or Diagenode, C15410195), mouse anti-KI67 (1:200, Abcam, #AB15580), mouse anti-SOX2 (1:200, Santa Cruz; sc-365823), rabbit anti-pH3 (1:300, Abcam, #AB5176), rat anti-TBR2 (1:300, Invitrogen, #14-4875-82). Secondary antibodies were used at 1:500 (Life Technologies).

Cell cycle length

Cell cycle length experiment was conducted following previously published paradigm (*32*). Briefly, at t0 pregnant females were injected peritoneally with BrdU (10mg/ml; 50 µl/10g) then at t1h30 with EdU (5mg/ml; 50µl/10g) and at t2h embryos were collected.

At least 3 sections per brain at each stage were quantified. The cell-cycle and S-phase duration were determined as follow: S-phase = 1.5 x (SOX2$^+$BrdU$^+$EdU$^+$ / SOX2$^+$BrdU$^+$EdU$^-$); total cell cycle = S-phase x (SOX2$^+$/ SOX2$^+$EdU$^+$) (*32*).

Electrophysiology

Four hundred μm-thick coronal slices were prepared from E12.5, E13.5, E14.5, E15.5 and E16.5 CD1 mice embryos and kept 30 minutes at 33°C in artificial cerebrospinal fluid (aCSF) containing 125 mM NaCl, 2.5 mM KCl, 1 mM MgCl$_2$, 2.5 mM CaCl$_2$, 1.25 mM NaH$_2$PO$_4$, 26 mM NaHCO$_3$ and 11 mM glucose, saturated with 95% O$_2$ and 5% CO$_2$. Slices were then transferred in the recording chamber, submerged and continuously perfused with aCSF. The internal solution used for the experiments contained 140 mM potassium methansulfonate, 2 mM MgCl$_2$, 4 mM NaCl 0.2 mM EGTA, 10 mM HEPES, 3 mM Na$_2$ATP, 0.33 mM GTP and 5 mM creatine phosphate (pH 7.2, 295 mOsm). Cells in immediate proximity to the ventricular wall (*i.e.* putative APs) were patched and clamped at -70mV. A baseline stable holding current was first measured for 4 minutes, after which a 10-minute bath of 100 μM of the glutamate transporter antagonist DL-TBOA (DL-*threo*-β -Benzyloxyaspartate) (*52*) was applied and finally washed out. TBOA-induced currents were blocked by application of 25 μM NBQX and 50 μM D-APV (data not shown), consistent with activation of ionotropic glutamate receptors by increased extracellular levels of Glu (*52*). Recorded currents were amplified (Multiclamp 700, Axon Instruments), filtered at 5kHz, digitalized at 20kHz (National Instrument Board PCI-MIO-16E4, IGOR WaveMetrics), and stored on a personal computer for further analyses (IGOR PRO WaveMetrics). The net amplitude of TBOA induced currents was determined after subtraction of baseline holding current.

In vitro experiments

Embryos were injected with FT at E12 or E15 and collected 1 hour or 4 days after injection in ice-cold HBSS (Gibco; #14175-053). The dorsal pallium was microdissected under stereomicroscopic guidance (Leica, #M165 FC) using a microscalpel. Tissue from 5-6 littermates was pooled and incubated in 400 μl TrypLE (Gibco; #12605-010) for 5 minutes at 37°C. TrypLE was inactivated by adding HBSS containing 0.1% BSA and the tissue was mechanically dissociated by pipetting the suspension 6-8 times with a 1 ml pipette. Cells were filtered through a 70 μm cell strainer, centrifuged (150 rpm, 5 minutes) and resuspended in FACS buffer (L15 medium, Gibco; #21083-

027, containing 2 mg/ml glucose, 0.1% BSA, 1:50 citrate phosphate dextrose, 10 units/ml DNase I and 1 μM $MgCl_2$). The top 10% brightest FT positive cells were sorted on an S3e Cell Sorter (BioRad) or a BD FACS Aria II flow cytometer (BD Biosciences) and collected in ice-cold FACS buffer. Sorted cells were centrifuged (150 rpm, 5 minutes) and resuspended either in Neurobasal media (Gibco; #21103-049, supplemented with 500 mM Glutamax-I, 2% of B27 (Gibco; 17504-044), and 1% of penicillin/streptomycin antibiotic) or DMEM/F12 (Gibco; #31331-028, supplemented with 1× N2, Gibco; #A13707-01, FGF2; Sigma; #SRP4038-50UG, 2% of B27, and 1% of penicillin/streptomycin antibiotic). Sorted cells were plated on previously coated coverslips with poly-L-lysine (0.1mg/ml) and laminin (0.33μg/ml). Cells were maintained at 37° C with 5% CO_2 for 2 hours (*in vivo* arm) or 4 days *in vitro*. Following BRN2 and CTIP2 immunostaining, cells were imaged and the fluorescence intensity in the nucleus was calculated for both markers using R software. Cells with an intensity value for both markers below 25% to the maximum intensity per condition and cells with saturated intensity values for both markers were not considered for analysis. To mitigate potential artefactual staining, the thresholds were determined based on the *in vivo* condition: for the quantifications in fig. S8B, cells with a CTIP2/BRN2 ratio above 2.5 were considered as CTIP2^{+} while cells with a CTIP2/BRN2 ratio below 1 were considered as BRN2^{+}.

Cell cycle exit

Pregnant females at E14.5 or E15.5 were injected i.p by a single pulse of EdU (1mg/ml; 50μl/10g) and embryos were collected 24 hours later. At least 3 sections per brain in each condition ($n = 3$ brains/condition) were quantified. The cell cycle exit rate was determined by dividing the number of KI67^{+}EdU[+] by the total number of EdU^{+} cells.

Sm-FISH

Twelve μm-thick coronal sections were prepared from fresh frozen embryonic brains at E12, E13, E14 and E15 and incubated at room temperature for 1 hour. Sections were then fixed with 4% PFA for 15 min and processed according to the manufacturer's instructions, using the RNAscope Multiplex Fluorescent kit (Advanced Cell Diagnostics) for fresh frozen tissue. Briefly, sections were dehydrated using 50%, 70% and 100% successive baths of ethanol. A 10 min treatment in SDS (4% in 200 mM sodium borate) was added in the protocol after Protease IV incubation as

proposed in (*9*). The probes were then incubated on sections during 2 hours at 40°C and processed for amplification steps. Finally, sections were counterstained with DAPI and mounted with Mowiol medium. The following probes were used: *Nes* (Acdbio, #313161-C3), *Fn1* (Acdbio, #316951-C2) and *Clu* (Acdbio, #427891). For quantifications, images were processed using a custom script that identifies each molecule of mRNA and transformes it as a pixel. Pixels were then automatically counted in the VZ (delineated by the expression of Nestin mRNA). Three embryos per age were analyzed.

Imaging

Images were acquired using a LSM 700 confocal laser scanning microscope (Carl Zeiss), a Nikon A1r spectral line scan confocal or an inverted LSM800 confocal microscope (Carl Zeiss). For brain sections, the putative primary somatosensory (S1) cortex was used as a region of study. The Zeiss Zen Blue, ImageJ, Photoshop (Adobe) and R softwares were further used for downstream image processing and analyses.

Quantifications

In fig. S1B top, % $SOX2^+KI67^+/FT^+$ was calculated, with an $n = 3$ for each stage. Values ± SEM are: E12: 98.6 ± 1.5; E13: 96.2 ± 1.9; E14: 98.9 ± 1.11; E15: 98.6 ± 1.11. In fig. S1B bottom, % $TBR2^+KI67^+/TBR2^+$ was calculated. Values ± SEM are: E12: 71.7 ± 6.3; E13: 79.2 ± 7.5; E14: 56.0 ± 17.5; E15: 16.8 ± 5.9.

In Fig. 2H, S-phase and total cell cycle length were calculated as mentioned above, with an $n = 3$ for each stage. For S-phase, values ± SEM are: E12: 4.3 ± 0.24; E13: 3.5 ± 0.6; E14: 3.7 ± 0.4; E15: 4.3 ± 0.4. For total cell cycle length, values ± SEM are: E12: 8.6 ± 0.3; E13: 9.4 ± 1.11; E14: 10.8 ± 1.1; E15: 12.0 ± 1.0. The values ± SEM for the fraction of S-phase APs in fig. S9C are: E12: 49.5 ± 1.1; E15: 35.7 ± 0.6.

In Fig. 2I, the net amplitude of GLAST-induced current was calculated. Values ± SEM are: E12: 1.6 ± 0.8 ($n = 6$); E13: 1.2 ± 0.8 ($n = 10$); E14: 2.6 ± 0.9 ($n = 8$); E15: 6.7 ± 2.4 ($n = 6$); E16: 24.8 ± 4.6.

In fig. S8B, % of $BRN2^+$ and $CTIP2^+$ cells were calculated as mentioned above. For the *in vivo* dataset (E12 $n = 2$; E15 $n = 3$), values ± SEM are: E12, $BRN2^+$: 88.1 ± 7.0; E12, $CTIP2^+$: 11.9 ±

7.0; E15, BRN2$^+$: 99.8 ± 0.1; E15, CTIP2$^+$: 0.40 ± 0.03. For the *in vitro* dataset (*n* = 3 per stage), values ± SEM are: E12, BRN2$^+$: 92.0 ± 6.2; E12, CTIP2$^+$: 12.1 ± 8.1; E15, BRN2$^+$: 99.6 ± 0.4; E15, CTIP2$^+$: 1.3.

In Fig. 6A (H3K27me3 staining) the H3K27me3 image intensity range was normalized to the brightest juxtaventricular VZ cells at each embryonic age.

In Fig. 6C, VZ thickness delimited by the SOX2 staining was calculated (*n* = 3 brains per condition). Values ± SEM are: E14 WT: 97.8 ± 1.2; E14 Eed cKO: 78.5 ± 0.6; E15 WT: 84.7 ± 0.9.

In Fig. 6D, cell cycle exit rate was calculated as mentioned above (*n* = 3 brains per condition). Values ± SEM are: E14 WT: 6.2 ± 0.6; E14 Eed cKO: 9.5 ± 0.8; E15 WT: 17.0 ± 1.0.

In Fig. 6E, % of BRN2$^+$/FT$^+$ cells was calculated (*n* = 3 brains per condition). Values ± SEM are: WT: 36.8 ± 2.6; Eed cKO: 53.4 ± 4.8.

In situ hybridization image processing

All *in situ* hybridizations were retrieved from the Allen Developing Mouse Brain Atlas (www.brain-map.org) and uniformly zoomed to the putative S1 neocortical region. For the illustrations in Fig. 1E and figs. S3, S6C and S7C, the images were aligned and stacked. The mean intensity level of the Z projection was calculated on ImageJ and the resulting layout was artificially colored using the "Fire" mode of ImageJ. In fig. S6C, semi-quantifications were performed by assigning a score to the strength of the signal in the juxtaventricular VZ (0 = absent, 1 = weak, 2 = medium, 3 = strong) for each gene. Genes were then grouped into early (*i.e.* belonging to dynamics 1-3) or late (*i.e.* belonging to dynamics 4-6) dynamics types and scores were averaged and normalized to the highest value across embryonic age. This scoring was performed blindly with regard to the gene identity.

scRNAseq experiment

Cell dissociation and FAC-sorting: Pregnant females were sacrificed either 1, 24 or 96 hours after FT injection. As previously described (*13*), embryonic brains were extracted in ice-cold HBSS, embedded in 4% agar low-melt and sectioned coronally at 300 µm using a vibrating microtome (Leica, #VT100S). The putative S1 cortical region was microdissected under a

stereomicroscope and incubated in 0.05% trypsin at 37°C for 5 minutes. Following tissue digestion, fetal bovine serum was added to the mix and cells were manually dissociated via up-and-down pipetting. Cells were centrifuged 5 min at 300 G and the pellet was suspended in 1 ml of HBSS then passed on a 70 µm cell strainer. FT^{+} cells, gated to include only the top 5% brightest cells (12,13), were finally FAC-sorted on a MoFloAstrios device (Beckman).

Single-cell RNA capture and sequencing: FAC-sorted FT^{+} cells (18 µl) were mixed with the C1 Suspension Reagent (2 µl; Fluidigm) yielding a total of 20 µl of cell suspension mix with ~500 cells / µl. The cell suspension mix was loaded on a C1 Single-Cell AutoPrep integrated fluidic circuit (IFC) designed for 10- to 17-µm cells (HT-800, Fluidigm #100-57-80). Batch effects were mitigated by distributing cells in the different conditions within single chips (*i.e.* E12 with E14 and E13 with E15) and by normalizing the number of reads per chip. cDNA synthesis and preamplification was processed following the manufacturer's instructions (C1 system, Fluidigm) and captured cells were imaged using the ImageXpress Micro Widefield High Content Screening System (Molecular Devices®). Single cell RNA-sequencing libraries of the cDNA were prepared using Nextera XT DNA library prep kit (Illumina). Libraries were multi-plexed and sequenced according to the manufacturer's recommendations with paired-end reads using HiSeq2500 plat-form (Illumina) with an expected depth of 1M reads per single cell, and a final mapping read length of 70 bp. All the single cell RNA capture and sequencing experiments were performed within the Genomics Core Facility of the University of Geneva.

The sequenced reads were aligned to the mouse genome (GRCm38) using the read-mapping algorithm TopHat. Unique Molecular Identifiers (UMI) sequenced in the first reads were used to correct for cDNA PCR amplification biases. Duplicated reads were identified and corrected using the deduplication step from the UMI-tools algorithm (53). The number of reads per transcript was calculated with the open-source HTSeq Python library. All the analyses were computed on the Vital-It cluster administered by the Swiss Institute of Bioinformatics.

scRNAseq analysis

Cell filtering: Doublet cells identified on the Fluidigm C1 plate images were excluded before initial analysis. A total of 2,906 FT^{+} single cells were obtained (**FT [+]1 h**: E12: 202 cells, E13: 211, E14: 135, E15: 304; **FT [+]24 h:** E12: 284 cells, E13: 286, E14: 232, E15: 217; **FT [+] 96 h:** E12: 246 cells, E13: 278, E14: 262, E15: 249). Cells expressing < 1000 genes or > 17% of mitochondrial

genes were excluded. After this step, 2,756 cells remained for analysis (**FT $^+$1 h**: E12: 189 cells, E13: 207, E14: 134, E15: 301; **FT $^+$24 h:** E12: 268 cells, E13: 223, E14: 219, E15: 213; **FT $^+$96 h**: E12: 244 cells, E13: 267, E14: 254, E15: 237).

Type specific transcripts: The AP, BP and N score used in Fig. 1B correspond to the mean transcript expression of the top 20 genes for AP, BP and N previously characterized (*12*): **AP**: *Aldoc, Pdpn, Vim, Ednrb, Ddah1, Ldha, Peg12, Wwtr1, Tspan12, Mfge8, Uhrf, Ncaph, Ndrg2, Mt1, Hk2, Psat1, Sp8, Sdc4, Dnmt3a, Notch2, Psph*. **BP**: *Btg2, Eomes, Abcg1, Kif26b, Mfap4, Coro1c, Myo10, Mfng, Rprm, Chd7, Ezr, Gadd45g, Slc16a2, Heg1, Celsr1, Tead2, Cd63, Rhbdl3, Mdga1, Arrdc3*. **N**: *Myt1l, Unc5d, 1700080N15Rik, Nos1, Satb2, Ank3, Scn3a, Dscam, Cntn2, Plxna4, 9130024F11Rik, Lrrtm4, Ptprk, Nrp1, Celsr3, Rbfox1, Flrt2, Kcnq3, Kcnq2, Gm36988.*

Clustering analysis was performed using the Seurat bioinformatics pipeline (https://github.com/satijalab/seurat) and is summarized here. We first created a "Seurat object" including all 2,756 cells and all genes. To remove sequencing depth biases between cells, we normalized and scaled the UMI counts using the *NormalizeData* (normalization.method = "LogNormalize", scale.factor = 100000) combined with the *ScaleData* function (vars.to.regress = c("nGene","nUMI")). A cell cycle phase was further assigned to each single cell using the Seurat pipeline. Gene expression was not normalized with regard to the cell cycle phase as this process is physiologically relevant in the temporal progression of cortical progenitors identity. We then determined the most variable genes by plotting transcripts into bins based on X-axis (average expression) and Y-axis (dispersion). This identified 4,016 transcripts. Parameters and cutoffs were set as follow: mean.function = ExpMean, dispersion.function = LogVMR, x.low.cutoff = 0.1, x.high.cutoff = 8, y.cutoff = 0.7. Next, we identified the statistically significant principal components and used the top 20 as input for t-Distributed Stochastic Neighbor Embedding dimensional reduction, using the *TSNEPlot* function. To identify cellular clusters, we adopted a graph-based clustering approach using *FindClusters* function with a 1.8 resolution. The robustness of the clustering was validated using an in-silico downsampling approach. Briefly, cells were randomly sampled down and re-clustered and the stability of the cellular cluster was estimated, and compared to a random clustering. Finally, a multiclass SVM model (implementation from R package *bmrm*) was trained on all cluster- assigned cells and genes were ranked according to their linear weights. For each class (*i.e.* clusters), genes with a significant linear weight (Z-test, FDR $\leq$ 0.05) were considered as enriched genes.

Pseudotime projection: APs, N1d and N4d cells at all embryonic ages identified in the cell clustering analysis were processed. Basal progenitors were not included in this analysis because N1d and N4d are overwhelmingly directly born from APs when using FT labeling (*12,13*). The pseudotime alignment method performed was previously described (*24*) and is summarized hereafter. In Fig. 2 and figs. S5 and S6, we restricted the datasets to the high variable genes (*n* = 4,016) and performed dimensionality reduction using the prcomp function of R software. Taking into consideration the significant principal components (PCs) explaining at least 2% of the total variance and using the R package princurve, we fitted a curve that described the maturation route (*i.e.* pseudo-birthdate or pseudo-differentiation) along which cells are organized. The beginning of the curve was established as the side where cell expressing the highest level of *Sox2* (AP) for pseudo-differentiation or the highest level of *Hmga2* (E12) for pseudo-birthdate. A maturation score reflecting the distance between the beginning of the curve and the cell was attributed to each cell and normalized between 0 to 1. This pseudotime alignment method was also validated on the AP population using the Monocle bioinformatic pipeline (*14*).We then restricted the dataset to the top 500 genes for each PCs and performed a "Partitioning Around Medoids" analysis using the PAM R package (K = 6, span = 0.6) and each gene expression dynamics was normalized between -1 and 1 to identify clusters of transcripts with similar dynamics along the pseudo-differentiation (Fig. 2A, fig. S5) or pseudo-birthdate (Fig. 2D, fig. S6). This approach was previously described elsewhere (*24*).

Ordinal regression models: We used a regularized ordinal regression method to predict on one hand the birthdate and on the other hand the differentiation status of each cell. We restricted the analysis to the high variable genes (*n* = 4,016) defined earlier. As the cells are expected to be organized within a differentiation and a birthdate continuum, we used and adapted a previously described ordinal regression model (*54*) implemented in the *bmrm* R package. In our context, a single linear model is optimized to predict cell differentiation status irrespectively of the date of birth and conversely. The linear weight of the models is used to rank the genes according to their ability to predict each cell category and the best 100 genes (top 50 and bottom 50) in each model were considered. The ordinal regression models were then re-optimized on these subsets of genes. In the ordinal regression model, the prediction scores are defined by the linear combination of the core genes expression. Since the values of the prediction score *per se* are arbitrary, the minimum and maximum values were replaced with AP / E12 and N4d / E15, respectively, in the

differentiation and birthdate models. All reported predictions were obtained by 10-fold cross-validation. For the birthdate prediction of the human embryo neocortical cell dataset (*7*), we first isolated APs and newborn neurons using the annotations provided by the authors. The dataset was then restricted to the human orthologs of the birthdate core genes identified in the current study and the pseudo-birthdate of these cells was calculated using the aforementioned birthdate ordinal regression model. The expression dynamics of the ortholog core genes were plotted along this pseudo-birthdate for both APs and their newborn progeny.

Transcriptional maps (Fig. 5): Cells were organized on a 2D grid based on their birthdate and differentiation status score. For this purpose, the data were linearly adjusted so that the average predicted values for each cardinal feature was aligned on the relative knot of the grid. The gene expression at a given coordinate of the 2D space was further estimated as the average expression of its 15 nearest neighbors. All transcriptional landscapes were normalized to the maximum value. For low-level expression genes (maximum value < 1 log), the maximum value was artificially set to 1 log, which correspond to a baseline noise threshold. The transcriptional landscapes of the most variable genes ($n = 4{,}016$) were further clustered by projecting genes onto a 2D t-SNE space and submitted to a k-means clustering ($K = 12$). The average expression pattern was calculated for each cluster and the transcriptional maps of all remaining genes ($n = 12{,}425$) were correlated to these 12 patterns. Select examples in Fig. 5C correspond to genes directly assigned or most highly correlated to the corresponding cluster.

Softwares

All single cell RNA sequencing analysis were perfomed using the R software with publicly available packages. GeneGo portal (https://portal.genego.com) was used to investigate the enriched gene ontology processes in Fig. 2. Cytoscape platform (*55*) associated with its plugin (*56*) was used to construct the enrichment gene ontology processes network in supplementary fig. S10. For this purpose, the latest version of gene ontology (go-basic.obo) and gene association (gene_association.mgi) from the Gene Ontology Consortium website (www.geneontology.org) were given as input in Bingo. The string database (http://string-db.org) implemented in Cytoscape platform was used to determine the protein-protein interactions in figs S5, S6 and S7.

Table S1: Selection of characterized genes from the birthdate model

Gene symbol	Enriched in	Gene weight	Function	References (PMID)
Hmga2	Early	-6.25	DNA-binding, chromatin-related. KO in early-stage cortical progenitors reduces neurogenic potential	22797695 / 18957199
Tbr1	Early	-3.65	TF. Instructs the laminar location and identity of deep layer neurons	16858776 / 20615956
Top2a	Early	-3.36	DNA topoisomerase. KO leads to laminar dysruptions in the cerebral cortex	12773624
Bcl11b	Early	-3.13	CTIP2, a TF. Marker of L5B neurons	15664173 / 18678899
H2afz	Early	-2.91	Histone protein. KO results in enhanced proliferation of progenitors and reduced differentiation.	29294103
Gadd45g	Early	-2.78	DNA demethylation. Direct target of Pax6.	19521500
Hes1	Early	-2.58	Transcriptional repressor. Represses precocious neuronal commitment of cortical progenitors	10627606
Filip1	Early	-2.24	Filamin-interacting protein. Controls the radial migration of newborn cortical neurons	12055638
Sox5	Early	-2.15	TF. Control the timing of sequential generation of corticofugal neurons subtypes	18215621 / 18840685
Ptprz1	Late	2.73	Receptor tyrosine phosphatase. In human oRGs; development of OPCs.	26406371 / 21969550
Cttnbp2	Late	2.85	Dendritogenesis	23015759
Sparcl1	Late	2.88	Surface protein. Terminal migration of neurons. Astrocyte marker	14715135
Glra2	Late	2.91	Glycin receptor subunit. Regulates BP generation	24926615
Trim9	Late	3.02	Ubiquitin ligase. Netrin1 signaling-associated; regulates neuronal morphogenesis	28701345
Nr2f1	Late	3.09	TF, COUP-TFI. Neuronal differentiation	25476200
Trim2	Late	3.36	Regulates axonal mrophogenesis	20796172
Tnc	Late	3.86	Extracellular matrix protein. oRG marker	26406371
Chl1	Late	3.92	ECM and cell adhesion protein. Inhibits Erk1/2- MAPK signaling and reduces progenitor proliferation	15504324 / 20933598 / 18077678
Unc5d	Late	4.36	Netrin receptor. Expressed in L4 neurons; mediates neuronal survival	21216843 / 18469807
Sema3c	Late	5.36	Semaphorin. Required for migration of superficial layer neurons	26182416
Zbtb20	Late	7.04	Regulator for the generation of layer-specific neuronal identities; neuronal maturation	27282384 / 24828045

Table S2: Selection of characterized genes from the differentiation model

| Gene symbol	Enriched in	Gene weight	Function	References (PMID)
Vim	AP	-4.85	Intermediate filament protein. Classical marker of radial glia cells	Multiple references
Ccnd2	AP	-3.43	Cylin D2. Required for generation of BPs from APs	19641124
Chd7	AP	-3.17	Chromatin remodeler. Regulates AP proliferation; interacts with Sox2	27955690 / 21532573
Boc	AP	-3.10	SHH co-receptor. Regulates neuronal differentiation from cortical progenitor cells	27871935
Cdon	AP	-3.07	SHH co-receptor. Regulates cortical progenitor proliferation and neuronal differentiation	16648472
H2afz	AP	-2.98	Histone protein. KO results in enhanced proliferation of progenitors and reduced differentiation.	29294103
Hes1	AP	-2.88	Transcriptional repressor. Represses precocious neuronal commitment of cortical progenitors	10627606
Nes	AP	-2.65	Intermediate filament protein. Classical marker of radial glia cells	Multiple references
Rapgef6	AP	-2.59	GTPase. Reported to maintain the apical surface adherens junction in cortical progenitors.	27390776 / 28917843
Bcl11b	AP	-2.55	CTIP2, a TF. Marker of L5B neurons	15664173 / 18678899
Nfia	AP	-2.51	TF. Represses Notch pathway to initiate neuronal differentiation	20610746
Hmga2	AP	-2.31	DNA-binding, chromatin-related. KO in early-stage cortical progenitors reduces neurogenic potential	22797695 / 18957199
Qk	AP	-2.30	Involved in neuron-glia fate decisions	9778149
Arx	AP	-2.11	TF. Regulates AP proliferation and generation of BPs	23968833 / 18509041
Unc5d	N	3.06	Netrin receptor. Expressed in L4 neurons; mediates neuronal survival	21216843 / 18469807
Aff2	N	3.08	TF, transiently expressed in SVZ. Reported role in lymphcyte differentiation	12079280
Sparcl1	N	3.10	SVZ protein; obligatory binding partner of the neurite outgrowth-promoting factor pleiotrophin	28823557
Syt4	N	3.23	Syntaxin 4, retrograde synaptic signalling	23522040
Celf2	N	3.25	Regulation of RNA splicing	11158314
Nlgn3	N	3.28	Neuroligin 3, synaptic adhesion molecule	26235839
Sox11	N	3.30	TF, interacts with LHX2	28053041
Trim67	N	3.36	KO has CNS defects including decreased size of callosum	26235839
Nrxn1	N	3.37	Neurexin 1, synaptic protein	28013231
Zbtb18	N	3.40	Disruption of superficial cortical layers in KO	28053041
Dkk3	N	3.52	Wnt pathway inhibitor	18719393
Dpysl3	N	3.56	Axonal guidance and outgrowth	10504203
Bcl11a	N	3.63	TF. Controls the migration of cortical neurons with Sema3c; settles identity of corticofugal neurons	26182416 / 25972180
Sema3c	N	3.76	Semaphorin. Required for migration of superficial layer neurons	26182416
Neurod6	N	3.88	TF. Classical neuronal marker	Multiple references
Satb2	N	3.88	TF. Regulates differentiation of callosal projection neurons; mutually repressive interactions with Fezf2	26324926 / 25037921 / 18255031/ 18255030
Dcx	N	3.98	Microtubule associated protein. Critical for neuronal migration and proper cortical layering	10399932 / 10399933 / 14625554 / 12764037
Clstn2	N	4.11	Excitatory synapse transmission	12498782 / 28912692
Tuba1a	N	4.11	Tubulin-related. Mutation causes lisencephaly	20466733
Arpp21	N	4.23	RNA-binding; controls neuronal excitability and dendritic morphology in neocortex	29581509
Gpm6a	N	4.34	Neuronal differentiation and migration of neuronal stem cells	19298174
Smarca2	N	4.37	Chromatin-remodeling; activation of *Neurod2* and *Ngn*	11134956 / 15576411
Rtn1	N	4.38	ER-related; involved in neuronal differentiation; used as a marker	9560466
Neurod2	N	4.46	Neuronal specific genes, induces premature exit from cell cycle	26940868
Zbtb20	N	4.51	Regulator for the generation of layer-specific neuronal identities; neuronal maturation	27282384 / 24828045
Gria2	N	4.57	AMPA receptor subunit	Multiple references
Tubb3	N	4.63	Tubulin-related. Mutation causes abnormal cortical development	30016746
Mef2c	N	5.37	Activity-dependent TF. Regulates synaptogenesis	27989458
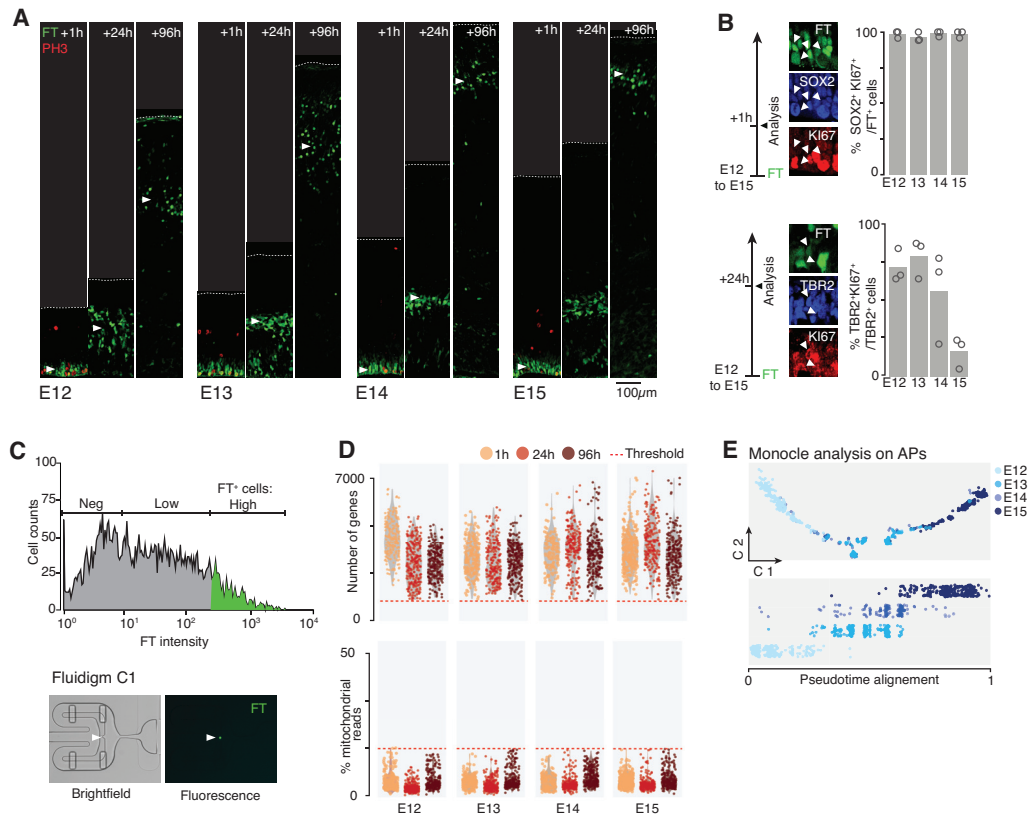
Fig. S1. scRNA sequencing of isochronic cohorts of cells in the developing neocortex. (A) FT injection labels isochronic cohorts of cortical cells which were collected either 1, 24 or 96 hours after labeling. E12 illustration modified from Fig.1. (B) Top: essentially all FT+ SOX2+ cells are proliferative (*i.e*. KI67+) at the FT+1h collection time point, throughout corticogenesis. Bottom: the fraction of proliferative TBR2+ cells (*i.e*. including intermediate progenitors) decreases with corticogenesis. (C) FT+ cells were FAC-sorted (top) and captured on a C1 microfluidic device (bottom) for scRNAseq processing. (D) Number of genes (top) and the percentage of mitochondrial genes (bottom) in each cell. Lower (< 1000 genes) and upper (> 17% mitochondrial genes) accepted thresholds are displayed. (E) Unbiased analysis of single-cell trajectories (Monocle) (14), highlighting the AP birth-date axis. Abbreviations: AP: apical progenitor, C: component, FT: Flashtag.
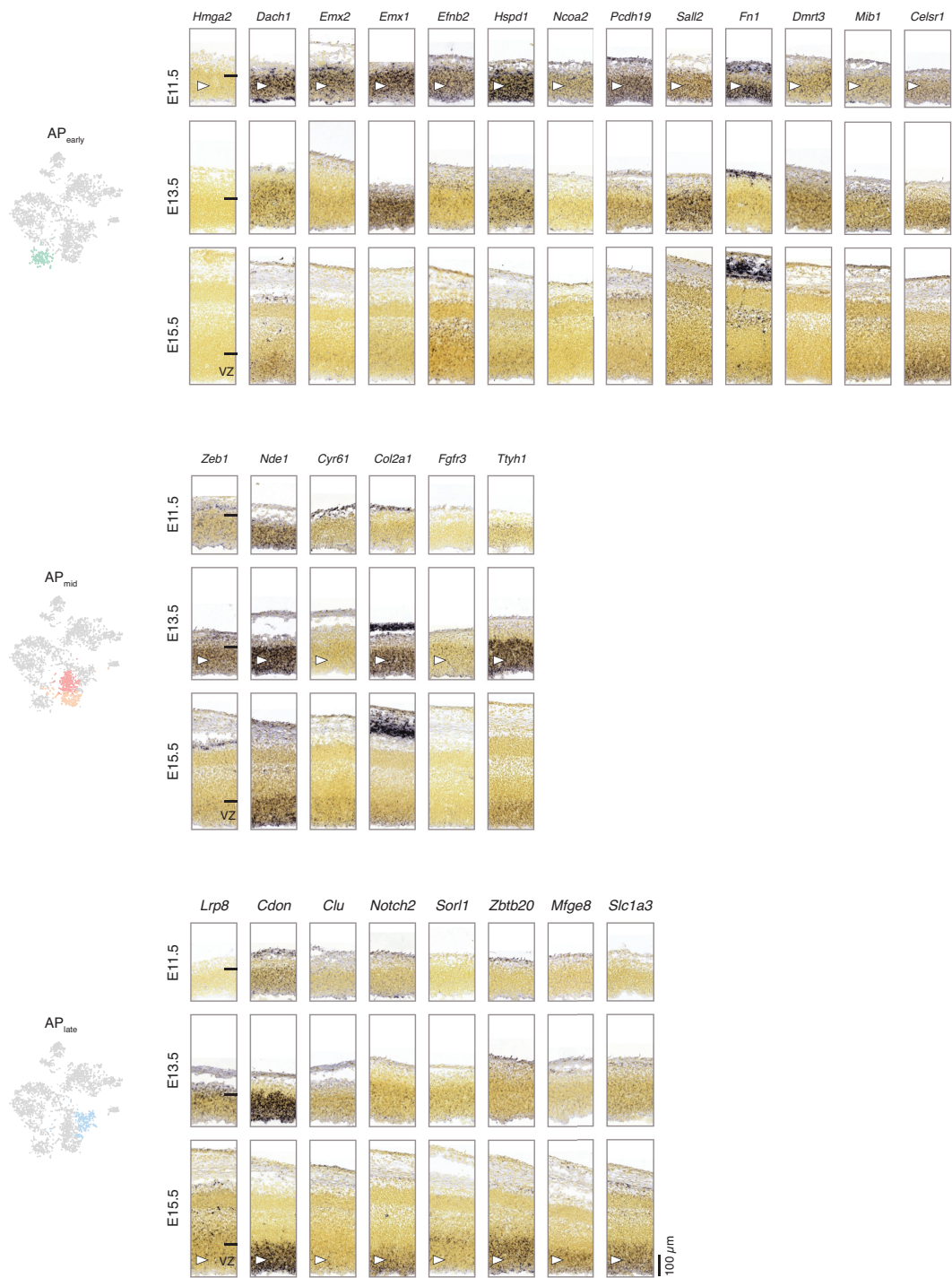
Fig. S2. Spatio-temporal expression of the most enriched genes in AP clusters. In situ hybridization of genes enriched in APearly, APmid, and APlate clusters. The ISH merged layouts are also presented in Fig. 1E. Tick mark indicates VZ basal border. Source of ISH: Allen Developing Mouse Brain Atlas. Abbreviations: AP: apical progenitor, VZ: ventricular zone.

Fig. S3. Spatio-temporal expression of the most enriched genes in 4-day-old clusters. Individual and merged in situ hybridization of genes enriched in N4dearly1, N4dearly2, N4dlate1 and N4dlate2 clusters. The ISH merged layouts for N4dearly1 and N4dlate2 are also presented in Fig. 1E. Source of ISH: Allen Developing Mouse Brain Atlas. Abbreviations: CP: cortical plate, N4d: 4-day-old neurons.
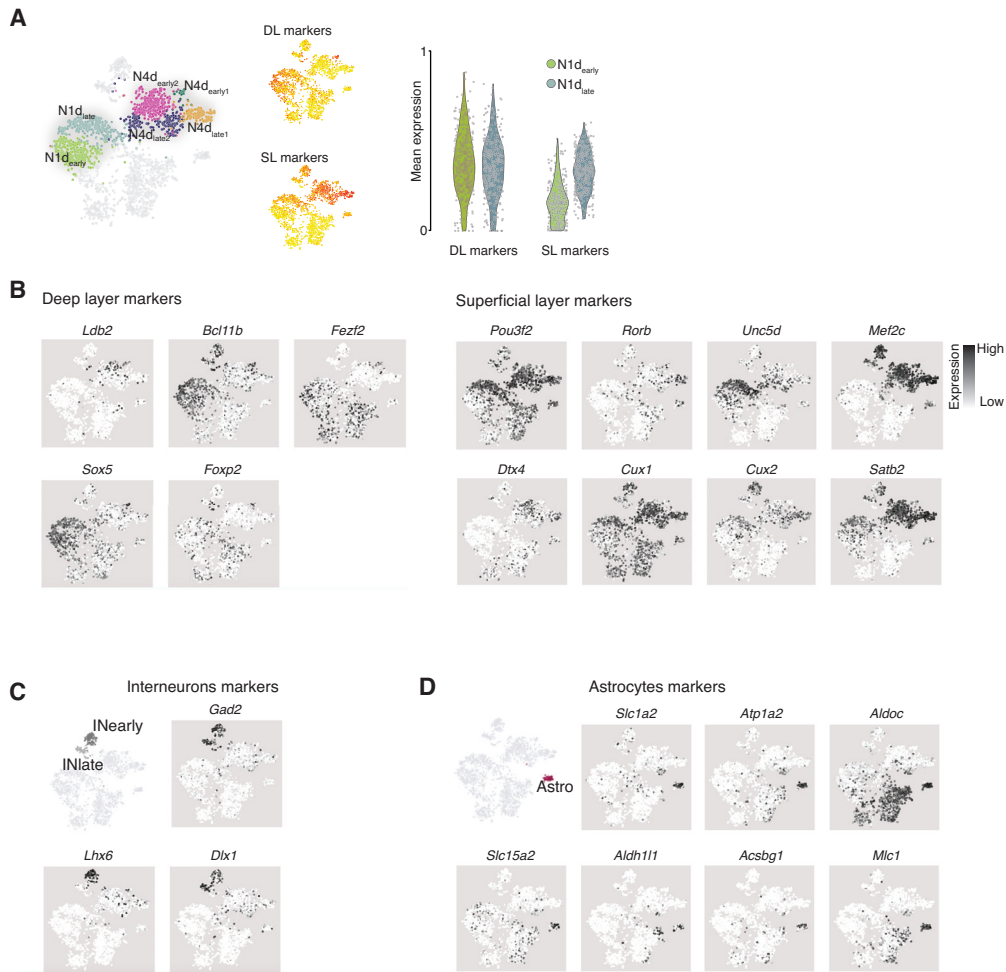
Fig. S4. Expression of select genes in neurons, astrocytes, and interneurons. (A) Feature plots showing expression of classical deep layer (DL) and superficial layer (SL) markers in 1-day and 4-day-old neurons across corticogenesis. Note that N1dlate neurons (*i.e.* E14 and E15-born neurons) initially and transiently express DL markers, as illustrated in the violin plots. (B) Expression of select laminar markers. (C) Expression of select ventral pallial-derived interneuron markers. (D) Expression of select astrocytes markers. Abbreviations: Astro: astrocytes, DL: deep layers, IN: interneurons, N1d: 1-day-old neurons, N4d: 4-day-old neurons, SL: superficial layers.
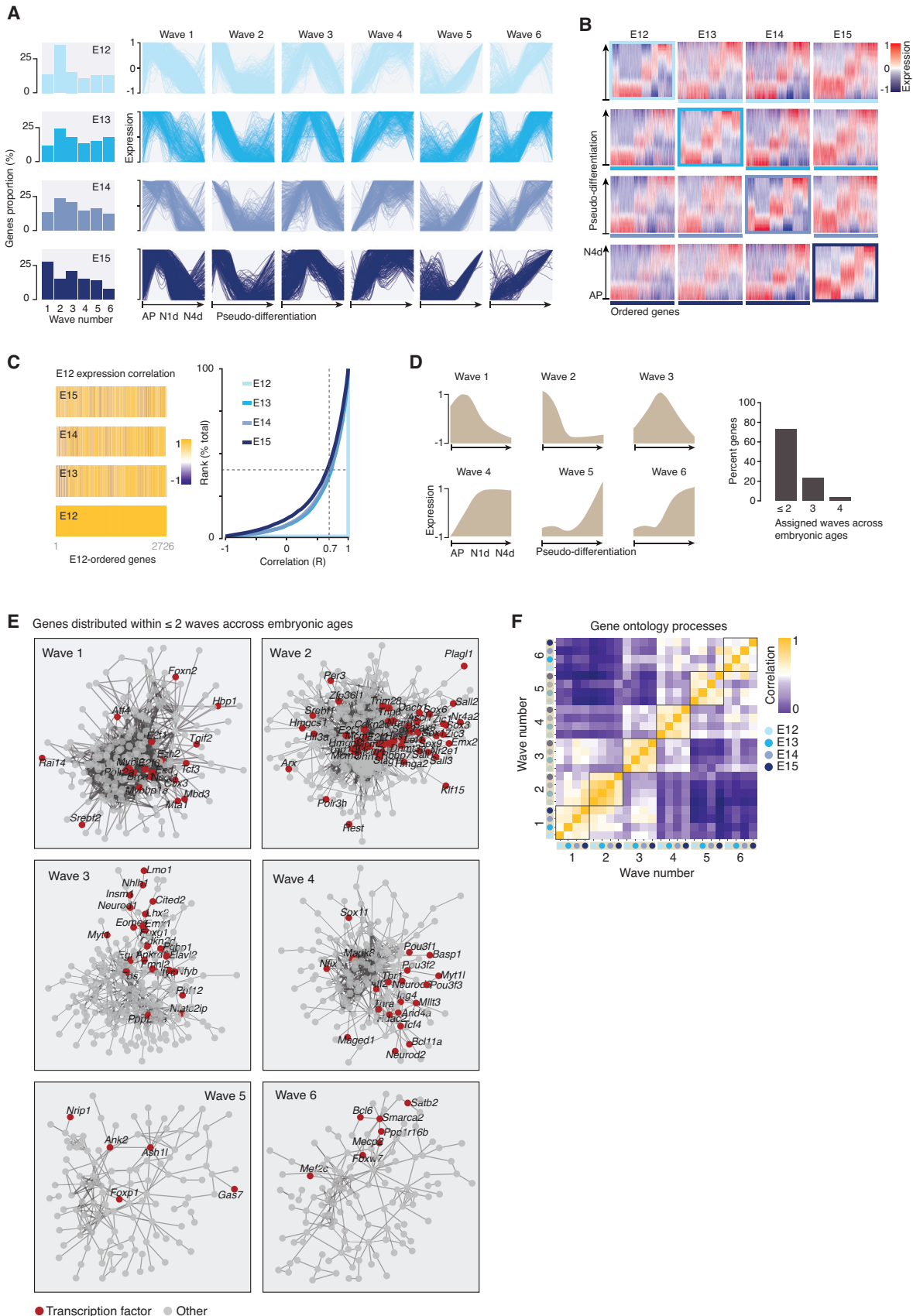
Fig. S5. Transcriptional differentiation waves at each embryonic age. (A) Gene distribution across the six differentiation waves at each embryonic age. (B) Gene waves at each embryonic age, organized by a reference sequence represented by a boxed area. (C) Left: Correlation of gene kinetics considering E12 as a reference shows that most gene expression dynamics are independent of the develop-mental age. Right: About half of the expressed genes had highly conserved expression dynamics. (D) Gene distribution within waves across embryonic ages. (E) Protein-protein interactome (from https://string-db.org/) of the most stable genes within each wave. Unassigned genes are not displayed. (F) Parallel progression of gene ontology processes associated with each transcription-al wave. Abbrevations: AP: apical progenitor, N4d: 4-day-old neurons.
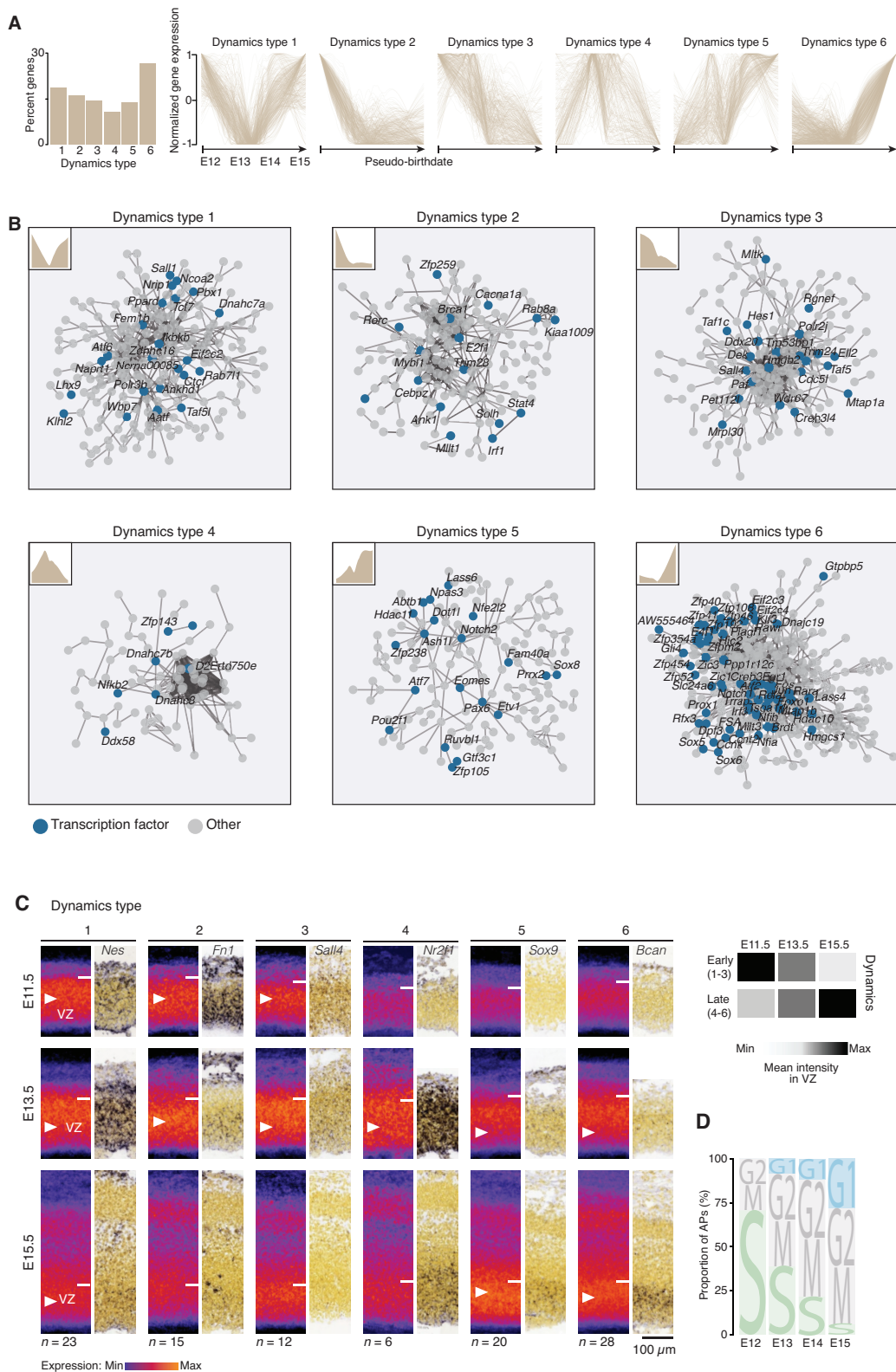
Fig. S6. Sequential AP transcriptional states across corticogenesis. (A) Normalized gene expressions are distributed within six sequential AP transcriptional states. (B) Global protein-protein interactome for each AP state, from https://string-db.org/. Unassigned genes are not displayed. (C) Sample and cumulative ISH hybridizations for all dynamically-expressed genes in the Allen Developing Mouse Brain Atlas. Righ: semi-quantifications of the ISH intensity in the VZ for the aggregate early (*i.e.* 1 to 3) and late (*i.e.* 4 to 6) dynamics. (D) The fraction of APs in G1 increases across corticogenesis as a result of the lengthening in t h e c e l l c y c l e , as reflected by expression of cell-cycle-enriched transcripts (see Methods for details). Abbreviations: AP: apical progenitor, VZ: ventricular zone.
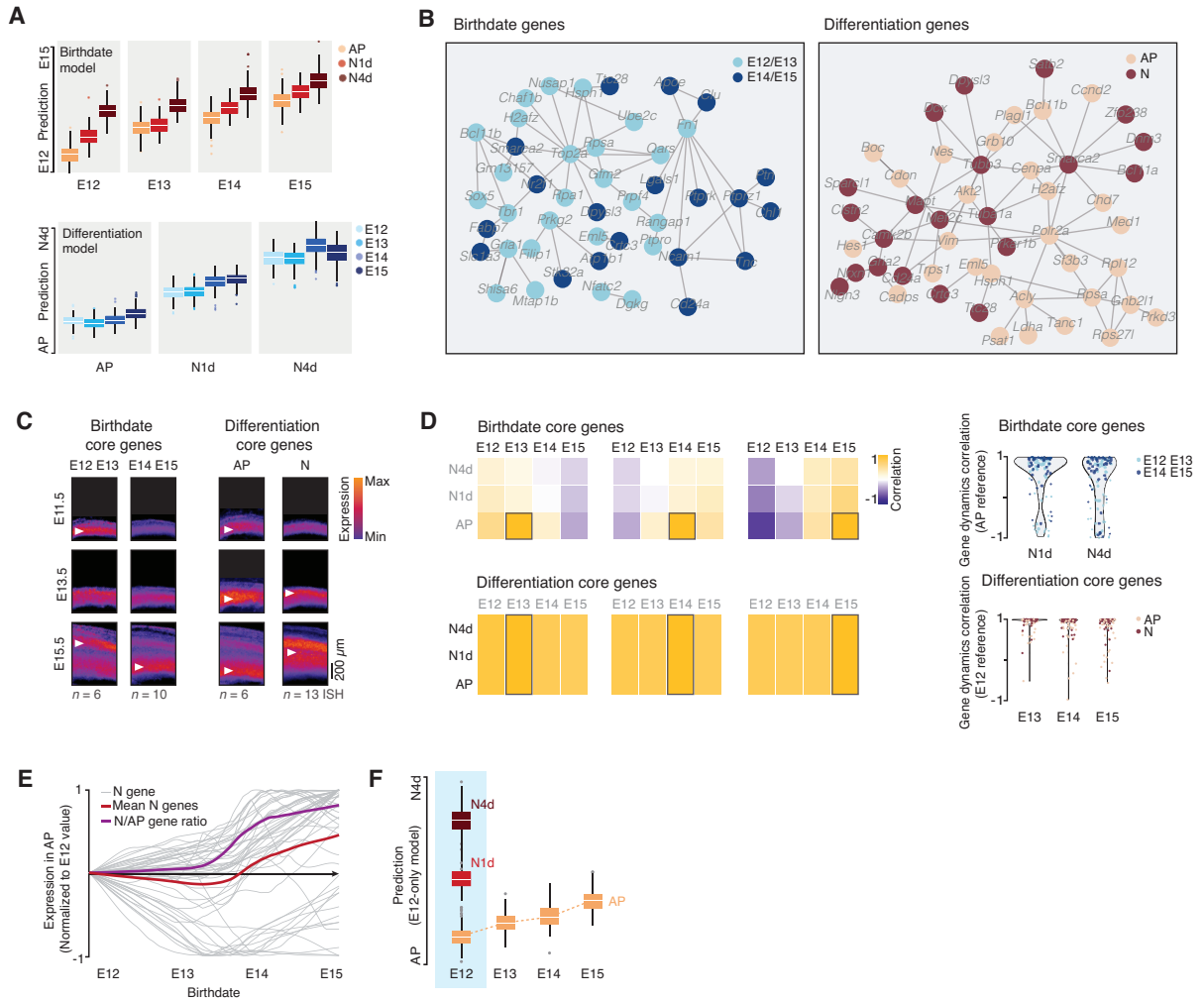
Fig. S7. 2D modelization of corticogenesis. (A) Birthdate and differentiation scores obtained from the two models for each condition. (B) Analysis of protein-protein interactions using the STRING database (http://string-db.org) suggests that gene products interact based on their temporal dynamics (left) or cellular specificity (right). Unassigned genes are not displayed. (C) Overlay of ISH from the Allen Developing Mouse Brain Atlas (www.brain-map.org) confirming the proper spatio-temporal dynamics of select core genes. Early genes: *Hes1, Hmga2, Tbr1, Fn1, Nfatc2, Sox5. Late genes: Nrxn1, Cttnbp2, Clu, Nr2f1, Lgals1, Bcan, Tnc, Unc5d, Slc1a3, Mfge8*. AP genes: *Cdon, Hes1, Plagl1, Nes, Hmga2, Arx. N genes: Trps1, Unc5d, Sox11, Nrxn, Cd24a, Mpped1, Bcl11a, Neurod6, Satb2, Dcx, Mapt, Gria2, Tubb3*. (D) Top left: Birthdate-associated core genes are temporally dynamic and daughter cells acquire embryonic stage-specific transcriptional birthmarks. Bottom left: In contrast, differentiation status-associated core genes are conserved across corticogenesis. Boxed area represents value of reference for correlation. Right: Correlations in gene expression dynamics stratified for early (E12, E13) and late (E14, E15) embryonic ages. (E) Expression of the core neuronal genes (*n* = 50) within APs increases with embryonic age. (F) E12-15 APs progressively become "neuronized". Differentiation model build exclusively with E12 data as a training dataset; E13-E15 APs are classified as progressively more neuron-like using this model. Abbreviations: AP: apical progenitor, N: neurons, N1d: 1-day-old neurons, N4d: 4-day-old neurons.
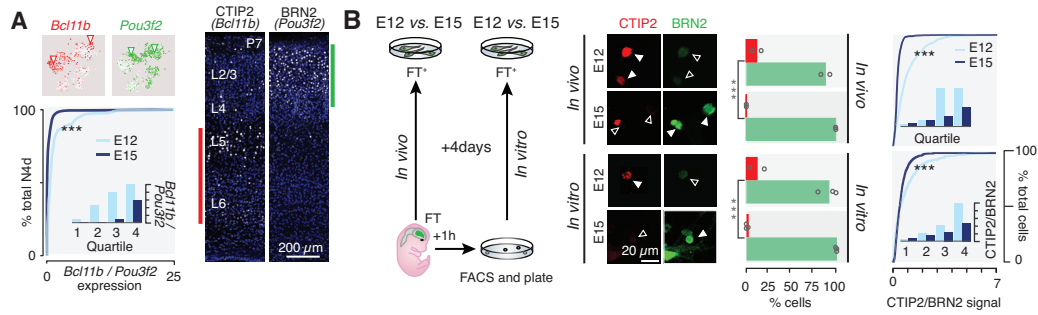
Fig. S8. Temporal patterning is still present in vitro. (A) The *Ctip2/Brn2* ratio (*i.e. Bcl11b/Pou3f2* ratio) is higher for E12-born neurons than for E15-born neurons. Top: feature plot showing expression levels, modified from S4B. Bottom: cumulative plots showing expression ratios in N4d. Right: CTIP2 and BRN2 proteins are expressed in DL and SL neurons, respectively. (B) Left: schematic of the experimental setup. In both the in vivo and in vitro arm, staining is performed on dissociated cells to allow for direct comparison of CTIP2 and BRN2 expression. Center and right: neurons born from E12 and E15 APs can still be distinguished by their relative expression of CTIP2 and BRN2 in vitro, as is the case in vivo. Abbreviations: FT: FlashTag, N4d: 4-day-old neurons. *** *P* < 0.001, Fisher's exact test (for bar graph); Kolmogorov-Smirnov test (for cumulative plots).
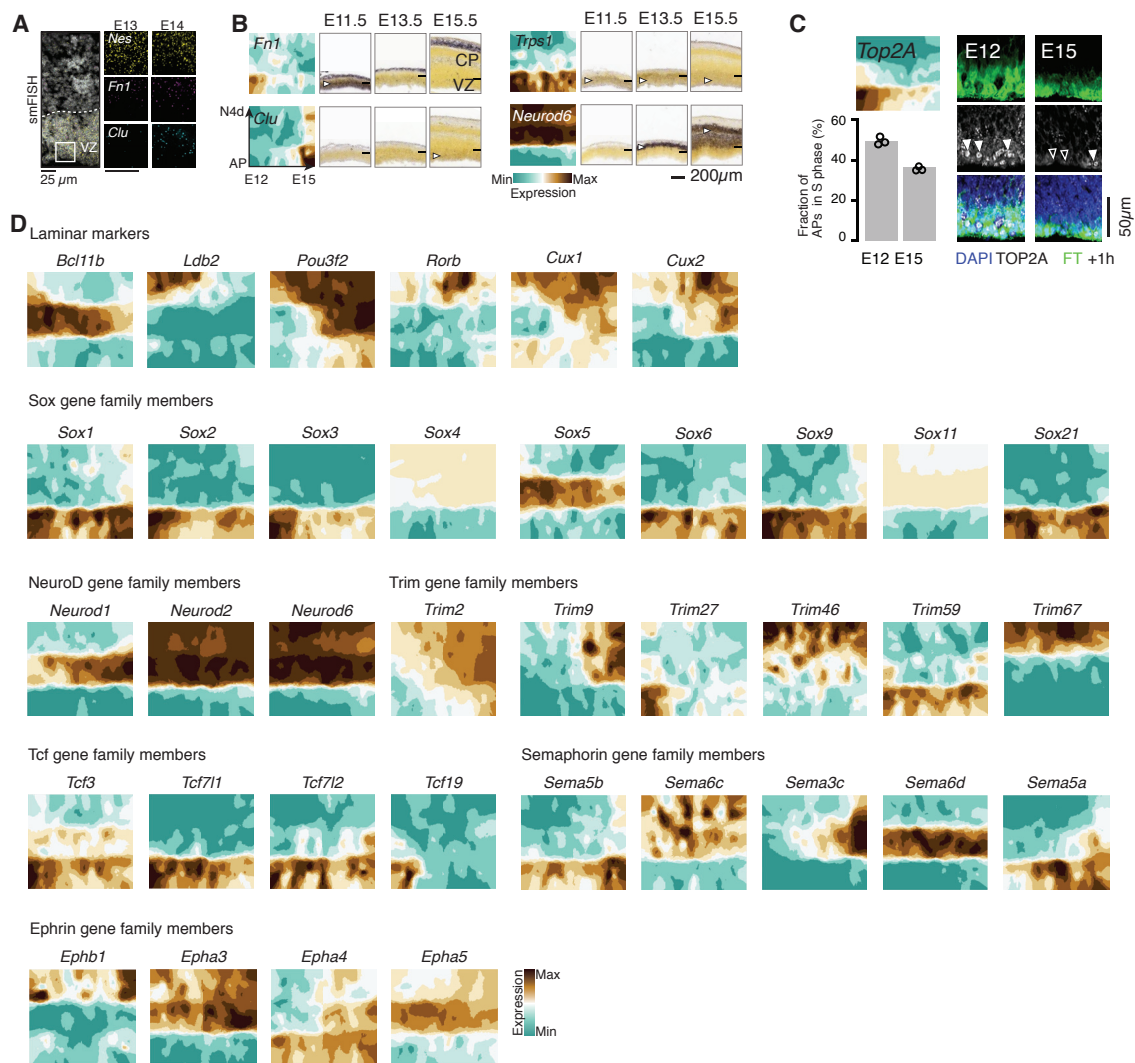
Fig. S9 Mapping of transcriptional dynamics in the developing cortex. Validation of select transcriptional patterns using (A) smFISH (see also Fig. 5B for E12 and E15 timepoints) (B) ISH from the Allen Developing Mouse Brain Atlas (www.brain-map.org) or (C) ICC. Of note, the decreased expression of *Top2A*, a S/G2-phase marker, in APs is consistent with a lengthening of the cell-cycle and a decreased proportion of S-phase APs between E12 and E15 (data from Fig. 2H analysis). (D) Transcriptional maps for select classical laminar markers and members of sample gene families. Only the genes with the most sharply delineated expression patterns are shown for Semaphorins and Ephrins. See www.genebrowser.unige.ch/telagirdon for more transcripts. Abbreviations: AP: apical progenitor, N4d: 4-day-old neurons.
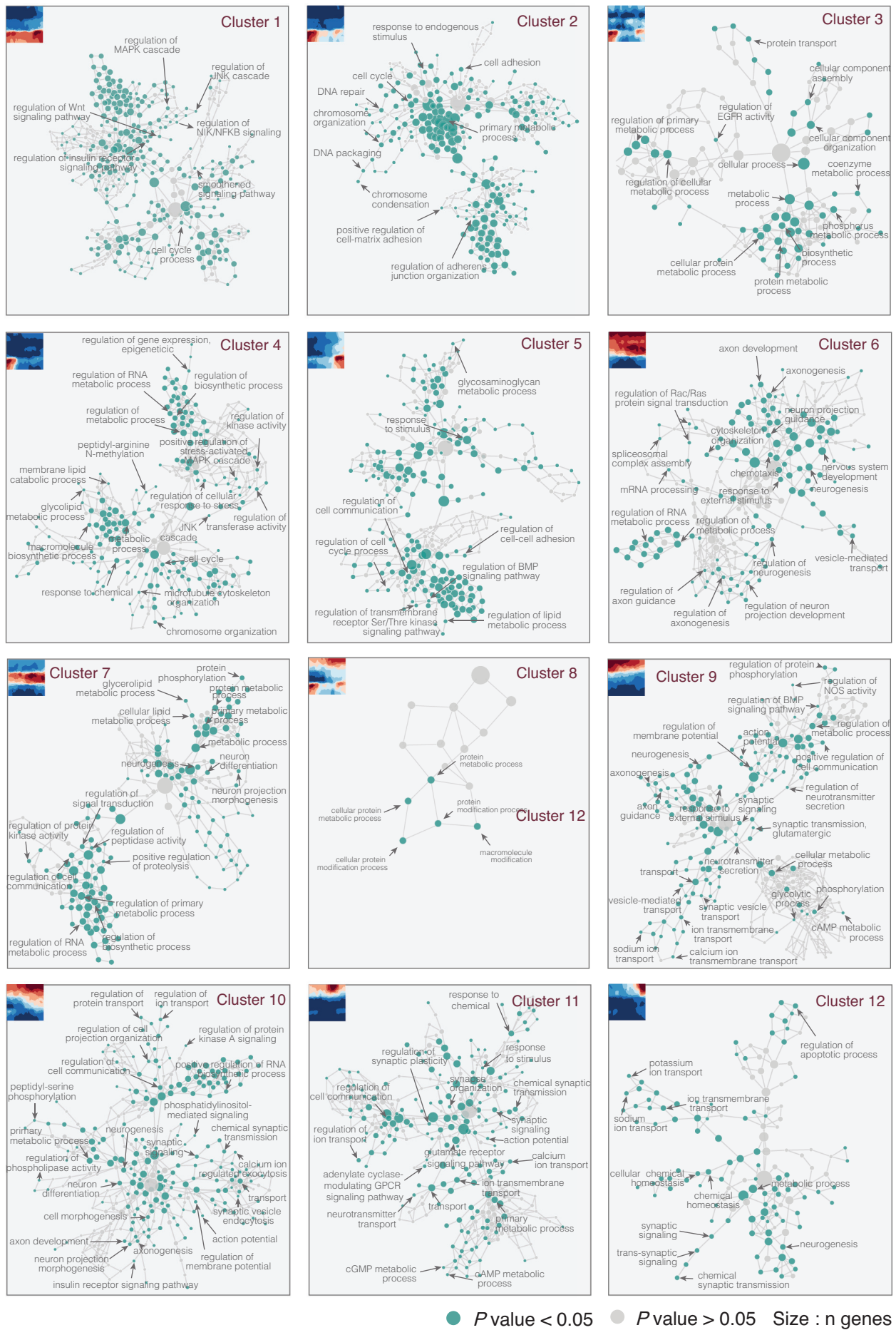
Fig. S10. Cluster-based gene ontology networks. Display of ontological hierarchies for individual clusters highlights cluster-specific biological processes.

Data S1: Top 10 enriched genes for each cell cluster (related to Fig. 1D).

Data S2: Differentiation waves gene list (related to Fig. 2B).

Data S3: Differentiation waves biological processes (related to Fig. 2B,C).

Data S4: AP gene dynamics list (related to Fig. 2E).

Data S5: AP gene dynamics biological processes (related to Fig. 2E,F).

Data S6: Core genes of the models (related to Fig. 3A).

Data S7: Clustering of transcriptional maps (related to Fig. 5C).

Data S8: Biological processes associated with transcriptional maps clusters (related to Fig. 5D).

References

1. N. Gaspard, T. Bouschet, R. Hourez, J. Dimidschstein, G. Naeije, J. van den Ameele, I. Espuny-Camacho, A. Herpoel, L. Passante, S. N. Schiffmann, A. Gaillard, P. Vanderhaeghen, An intrinsic mechanism of corticogenesis from embryonic stem cells. *Nature* **455**, 351–357 (2008). doi:10.1038/nature07287 Medline

2. M. Okamoto, T. Miyata, D. Konno, H. R. Ueda, T. Kasukawa, M. Hashimoto, F. Matsuzaki, A. Kawaguchi, Cell-cycle-independent transitions in temporal identity of mammalian neural progenitor cells. *Nat. Commun.* **7**, 11349 (2016). doi:10.1038/ncomms11349 Medline

3. D. Jabaudon, Fate and freedom in developing neocortical circuits. *Nat. Commun.* **8**, 16042 (2017). doi:10.1038/ncomms16042 Medline

4. M. Kohwi, C. Q. Doe, Temporal fate specification and neural progenitor competence during development. *Nat. Rev. Neurosci.* **14**, 823–838 (2013). [doi:10.1038/nrn3618](doi:10.1038/nrn3618) Medline

5. A. Zeisel, A. B. Muñoz-Manchado, S. Codeluppi, P. Lönnerberg, G. La Manno, A. Juréus, S. Marques, H. Munguba, L. He, C. Betsholtz, C. Rolny, G. Castelo-Branco, J. Hjerling-Leffler, S. Linnarsson, Cell types in the mouse cortex and hippocampus revealed by single-cell RNA-seq. *Science* **347**, 1138–1142 (2015). doi:10.1126/science.aaa1934 Medline

6. B. Tasic, V. Menon, T. N. Nguyen, T. K. Kim, T. Jarsky, Z. Yao, B. Levi, L. T. Gray, S. A. Sorensen, T. Dolbeare, D. Bertagnolli, J. Goldy, N. Shapovalova, S. Parry, C. Lee, K. Smith, A. Bernard, L. Madisen, S. M. Sunkin, M. Hawrylycz, C. Koch, H. Zeng, Adult mouse cortical cell taxonomy revealed by single cell transcriptomics. *Nat. Neurosci.* **19**, 335–346 (2016). [doi:10.1038/nn.4216](doi:10.1038/nn.4216) Medline

7. T. J. Nowakowski, A. Bhaduri, A. A. Pollen, B. Alvarado, M. A. Mostajo-Radji, E. Di Lullo, M. Haeussler, C. Sandoval-Espinosa, S. J. Liu, D. Velmeshev, J. R. Ounadjela, J. Shuga, X. Wang, D. A. Lim, J. A. West, A. A. Leyrat, W. J. Kent, A. R. Kriegstein, Spatiotemporal gene expression trajectories reveal developmental hierarchies of the human cortex. *Science* **358**, 1318–1323 (2017). doi:10.1126/science.aap8809 Medline

8. A. Saunders, E. Z. Macosko, A. Wysoker, M. Goldman, F. M. Krienen, H. de Rivera, E. Bien, M. Baum, L. Bortolin, S. Wang, A. Goeva, J. Nemesh, N. Kamitaki, S. Brumbaugh, D. Kulp, S. A. McCarroll, Molecular diversity and specializations among the cells of the adult mouse brain. *Cell* **174**, 1015–1030.e16 (2018). doi:10.1016/j.cell.2018.07.028 Medline

9. A. Zeisel, H. Hochgerner, P. Lönnerberg, A. Johnsson, F. Memic, J. van der Zwan, M. Häring, E. Braun, L. E. Borm, G. La Manno, S. Codeluppi, A. Furlan, K. Lee, N. Skene, K. D. Harris, J. Hjerling-Leffler, E. Arenas, P. Ernfors, U. Marklund, S. Linnarsson, Molecular

architecture of the mouse nervous system. *Cell* **174**, 999–1014.e22 (2018). doi:10.1016/j.cell.2018.06.021 Medline

10. B. Tasic, Z. Yao, L. T. Graybuck, K. A. Smith, T. N. Nguyen, D. Bertagnolli, J. Goldy, E. Garren, M. N. Economo, S. Viswanathan, O. Penn, T. Bakken, V. Menon, J. Miller, O. Fong, K. E. Hirokawa, K. Lathia, C. Rimorin, M. Tieu, R. Larsen, T. Casper, E. Barkan, M. Kroll, S. Parry, N. V. Shapovalova, D. Hirschstein, J. Pendergraft, H. A. Sullivan, T. K. Kim, A. Szafer, N. Dee, P. Groblewski, I. Wickersham, A. Cetin, J. A. Harris, B. P. Levi, S. M. Sunkin, L. Madisen, T. L. Daigle, L. Looger, A. Bernard, J. Phillips, E. Lein, M. Hawrylycz, K. Svoboda, A. R. Jones, C. Koch, H. Zeng, Shared and distinct transcriptomic cell types across neocortical areas. *Nature* **563**, 72–78 (2018). doi:10.1038/s41586-018-0654-5 Medline

11. J. Kageyama, D. Wollny, B. Treutlein, J. G. Camp, ShinyCortex: Exploring single-cell transcriptome data from the developing human cortex. *Front. Neurosci.* **12**, 315 (2018). doi:10.3389/fnins.2018.00315 Medline

12. L. Telley, S. Govindan, J. Prados, I. Stevant, S. Nef, E. Dermitzakis, A. Dayer, D. Jabaudon, Sequential transcriptional waves direct the differentiation of newborn neurons in the mouse neocortex. *Science* **351**, 1443–1446 (2016). doi:10.1126/science.aad8361 Medline

13. S. Govindan, P. Oberst, D. Jabaudon, In vivo pulse labeling of isochronic cohorts of cells in the central nervous system using FlashTag. *Nat. Protoc.* **13**, 2297–2311 (2018). doi:10.1038/s41596-018-0038-1 Medline

14. C. Trapnell, D. Cacchiarelli, J. Grimsby, P. Pokharel, S. Li, M. Morse, N. J. Lennon, K. J. Livak, T. S. Mikkelsen, J. L. Rinn, The dynamics and regulators of cell fate decisions are revealed by pseudotemporal ordering of single cells. *Nat. Biotechnol.* **32**, 381–386 (2014). doi:10.1038/nbt.2859 Medline

15. S. A. Yuzwa, M. J. Borrett, B. T. Innes, A. Voronova, T. Ketela, D. R. Kaplan, G. D. Bader, F. D. Miller, Developmental emergence of adult neural stem cells as revealed by single-cell transcriptional profiling. *Cell Rep.* **21**, 3970–3986 (2017). doi:10.1016/j.celrep.2017.12.017 Medline

16. E. Azim, S. J. Shnider, G. Y. Cederquist, U. S. Sohur, J. D. Macklis, Lmo4 and Clim1 progressively delineate cortical projection neuron subtypes during development. *Cereb. Cortex* **19** (suppl. 1), i62–i69 (2009). doi:10.1093/cercor/bhp030 Medline

17. S. K. Zahr, G. Yang, H. Kazan, M. J. Borrett, S. A. Yuzwa, A. Voronova, D. R. Kaplan, F. D. Miller, A translational repression complex in developing mammalian neural stem cells that regulates neuronal specification. *Neuron* **97**, 520–537.e6 (2018). doi:10.1016/j.neuron.2017.12.045 Medline

18. O. Marín, Cellular and molecular mechanisms controlling the migration of neocortical interneurons. *Eur. J. Neurosci.* **38**, 2019–2029 (2013). doi:10.1111/ejn.12225 Medline

19. B. Wamsley, G. Fishell, Genetic and activity-dependent mechanisms underlying interneuron diversity. *Nat. Rev. Neurosci.* **18**, 299–309 (2017). [doi:10.1038/nrn.2017.30](doi:10.1038/nrn.2017.30) Medline

20. B. Nadarajah, J. G. Parnavelas, Modes of neuronal migration in the developing cerebral cortex. *Nat. Rev. Neurosci.* **3**, 423–432 (2002). [doi:10.1038/nrn845](doi:10.1038/nrn845) Medline

21. Y. Yokota, H. T. Gashghaei, C. Han, H. Watson, K. J. Campbell, E. S. Anton, Radial glial dependent and independent dynamics of interneuronal migration in the developing cerebral cortex. *PLOS ONE* **2**, e794 (2007). doi:10.1371/journal.pone.0000794 Medline

22. J. D. Cahoy, B. Emery, A. Kaushal, L. C. Foo, J. L. Zamanian, K. S. Christopherson, Y. Xing, J. L. Lubischer, P. A. Krieg, S. A. Krupenko, W. J. Thompson, B. A. Barres, A transcriptome database for astrocytes, neurons, and oligodendrocytes: A new resource for understanding brain development and function. *J. Neurosci.* **28**, 264–278 (2008). doi:10.1523/JNEUROSCI.4178-07.2008 Medline

23. S. Minocha, D. Valloton, Y. Arsenijevic, J.-R. Cardinaux, R. Guidi, J.-P. Hornung, C. Lebrand, Nkx2.1 regulates the generation of telencephalic astrocytes during embryonic development. *Sci. Rep.* **7**, 43093 (2017). doi:10.1038/srep43093 Medline

24. C. Mayer, C. Hafemeister, R. C. Bandler, R. Machold, R. Batista Brito, X. Jaglin, K. Allaway, A. Butler, G. Fishell, R. Satija, Developmental diversification of cortical inhibitory interneurons. *Nature* **555**, 457–462 (2018). doi:10.1038/nature25999 Medline

25. J. Nishino, I. Kim, K. Chada, S. J. Morrison, Hmga2 promotes neural stem cell self-renewal in young but not old mice by reducing p16Ink4a and p19Arf Expression. *Cell* **135**, 227–239 (2008). doi:10.1016/j.cell.2008.09.017 Medline

26. Y. Shimono, H. Murakami, Y. Hasegawa, M. Takahashi, RET finger protein is a transcriptional repressor and interacts with enhancer of polycomb that has dual transcriptional functions. *J. Biol. Chem.* **275**, 39411–39419 (2000). [doi:10.1074/jbc.M006585200](doi:10.1074/jbc.M006585200) Medline

27. C. L. Cunningham, V. Martínez-Cerdeño, S. C. Noctor, Microglia regulate the number of neural precursor cells in the developing cerebral cortex. *J. Neurosci.* **33**, 4216–4233 (2013). doi:10.1523/JNEUROSCI.3441-12.2013 Medline

28. I. Vitali, S. Fièvre, L. Telley, P. Oberst, S. Bariselli, L. Frangeul, N. Baumann, J. J. McMahon, E. Klingler, R. Bocchi, J. Z. Kiss, C. Bellone, D. L. Silver, D. Jabaudon, Progenitor Hyperpolarization Regulates the Sequential Generation of Neuronal Subtypes in the Developing Neocortex. *Cell* **174**, 1264–1276.e15 (2018). doi:10.1016/j.cell.2018.06.036 Medline

29. T. A. Weissman, P. A. Riquelme, L. Ivic, A. C. Flint, A. R. Kriegstein, Calcium waves propagate through radial glial cells and modulate proliferation in the developing neocortex. *Neuron* **43**, 647–661 (2004). doi:10.1016/j.neuron.2004.08.015 Medline

30. M. Knobloch, S. M. G. Braun, L. Zurkirchen, C. von Schoultz, N. Zamboni, M. J. Araúzo-Bravo, W. J. Kovacs, O. Karalay, U. Suter, R. A. C. Machado, M. Roccio, M. P. Lutolf, C. F. Semenkovich, S. Jessberger, Metabolic control of adult neural stem cell activity by Fasn-dependent lipogenesis. *Nature* **493**, 226–230 (2013). [doi:10.1038/nature11689](https://doi.org/10.1038/nature11689) [Medline](https://www.ncbi.nlm.nih.gov)

31. T. Takahashi, R. S. Nowakowski, V. S. Caviness Jr., The cell cycle of the pseudostratified ventricular epithelium of the embryonic murine cerebral wall. *J. Neurosci.* **15**, 6046–6057 (1995). [doi:10.1523/JNEUROSCI.15-09-06046.1995](https://doi.org/10.1523/JNEUROSCI.15-09-06046.1995) [Medline](https://www.ncbi.nlm.nih.gov)

32. B. Martynoga, H. Morrison, D. J. Price, J. O. Mason, Foxg1 is required for specification of ventral telencephalon and region-specific regulation of dorsal telencephalic precursor proliferation and apoptosis. *Dev. Biol.* **283**, 113–127 (2005). [doi:10.1016/j.ydbio.2005.04.005](https://doi.org/10.1016/j.ydbio.2005.04.005) [Medline](https://www.ncbi.nlm.nih.gov)

33. Y. Sela, N. Molotski, S. Golan, J. Itskovitz-Eldor, Y. Soen, Human embryonic stem cells exhibit increased propensity to differentiate during the G1 phase prior to phosphorylation of retinoblastoma protein. *Stem Cells* **30**, 1097–1108 (2012). [doi:10.1002/stem.1078](https://doi.org/10.1002/stem.1078) [Medline](https://www.ncbi.nlm.nih.gov)

34. A. Soufi, S. Dalton, Cycling through developmental decisions: How cell cycle dynamics control pluripotency, differentiation and reprogramming. *Development* **143**, 4301–4311 (2016). [doi:10.1242/dev.142075](https://doi.org/10.1242/dev.142075) [Medline](https://www.ncbi.nlm.nih.gov)

35. D. Jabaudon, K. Shimamoto, Y. Yasuda-Kamatani, M. Scanziani, B. H. Gähwiler, U. Gerber, Inhibition of uptake unmasks rapid extracellular turnover of glutamate of nonvesicular origin. *Proc. Natl. Acad. Sci. U.S.A.* **96**, 8733–8738 (1999). [doi:10.1073/pnas.96.15.8733](https://doi.org/10.1073/pnas.96.15.8733) [Medline](https://www.ncbi.nlm.nih.gov)

36. M. Eiraku, K. Watanabe, M. Matsuo-Takasaki, M. Kawada, S. Yonemura, M. Matsumura, T. Wataya, A. Nishiyama, K. Muguruma, Y. Sasai, Self-organized formation of polarized cortical tissues from ESCs and its active manipulation by extrinsic signals. *Cell Stem Cell* **3**, 519–532 (2008). [doi:10.1016/j.stem.2008.09.002](https://doi.org/10.1016/j.stem.2008.09.002) [Medline](https://www.ncbi.nlm.nih.gov)

37. G. Pouchelon, F. Gambino, C. Bellone, L. Telley, I. Vitali, C. Lüscher, A. Holtmaat, D. Jabaudon, Modality-specific thalamocortical inputs instruct the identity of postsynaptic L4 neurons. *Nature* **511**, 471–474 (2014). [doi:10.1038/nature13390](https://doi.org/10.1038/nature13390) [Medline](https://www.ncbi.nlm.nih.gov)

38. D. Jabaudon, S. J. Shnider, D. J. Tischfield, M. J. Galazo, J. D. Macklis, RORβ induces barrel-like neuronal clusters in the developing neocortex. *Cereb. Cortex* **22**, 996–1006 (2012). [doi:10.1093/cercor/bhr182](https://doi.org/10.1093/cercor/bhr182) [Medline](https://www.ncbi.nlm.nih.gov)

39. E. Klingler, A. De la Rossa, S. Fièvre, K. Devaraju, P. Abe, D. Jabaudon, A translaminar genetic logic for the circuit identity of intracortically projecting neurons. *Curr. Biol.* **29**, 332–339.e5 (2019). [doi:10.1016/j.cub.2018.11.071](https://doi.org/10.1016/j.cub.2018.11.071) [Medline](https://www.ncbi.nlm.nih.gov)

40. R. Margueron, D. Reinberg, The Polycomb complex PRC2 and its mark in life. *Nature* **469**, 343–349 (2011). doi:10.1038/nature09784 Medline

41. J. D. Pereira, S. N. Sansom, J. Smith, M.-W. Dobenecker, A. Tarakhovsky, F. J. Livesey, Ezh2, the histone methyltransferase of PRC2, regulates the balance between self-renewal and differentiation in the cerebral cortex. *Proc. Natl. Acad. Sci. U.S.A.* **107**, 15957–15962 (2010). doi:10.1073/pnas.1002530107 Medline

42. J. S. Dasen, Transcriptional networks in the early development of sensory-motor circuits. *Curr. Top. Dev. Biol.* **87**, 119–148 (2009). [doi:10.1016/S0070-2153(09)01204-6](doi:10.1016/S0070-2153(09)01204-6) Medline

43. D. Mi, Z. Li, L. Lim, M. Li, M. Moissidis, Y. Yang, T. Gao, T. X. Hu, T. Pratt, D. J. Price, N. Sestan, O. Marín, Early emergence of cortical interneuron diversity in the mouse embryo. *Science* **360**, 81–85 (2018). doi:10.1126/science.aar6821 Medline

44. L. Telley, D. Jabaudon, A mixed model of neuronal diversity. *Nature* **555**, 452–454 (2018). [doi:10.1038/d41586-018-02539-4](doi:10.1038/d41586-018-02539-4) Medline

45. K.-J. Yoon, F. R. Ringeling, C. Vissers, F. Jacob, M. Pokrass, D. Jimenez-Cyrus, Y. Su, N.-S. Kim, Y. Zhu, L. Zheng, S. Kim, X. Wang, L. C. Doré, P. Jin, S. Regot, X. Zhuang, S. Canzar, C. He, G. L. Ming, H. Song, Temporal control of mammalian cortical neurogenesis by m6a methylation. *Cell* **171**, 877–889.e17 (2017). doi:10.1016/j.cell.2017.09.003 Medline

46. K.-J. Yoon, C. Vissers, G.-L. Ming, H. Song, Epigenetics and epitranscriptomics in temporal patterning of cortical neural progenitor competence. *J. Cell Biol.* **217**, 1901–1914 (2018). [doi:10.1083/jcb.201802117](doi:10.1083/jcb.201802117) Medline

47. M. Z. Ozair, C. Kirst, B. L. van den Berg, A. Ruzo, T. Rito, A. H. Brivanlou, hPSC Modeling reveals that fate selection of cortical deep projection neurons occurs in the subplate. *Cell Stem Cell* **23**, 60–73.e6 (2018). doi:10.1016/j.stem.2018.05.024 Medline

48. T. J. Nowakowski, N. Rani, M. Golkaram, H. R. Zhou, B. Alvarado, K. Huch, J. A. West, A. Leyrat, A. A. Pollen, A. R. Kriegstein, L. R. Petzold, K. S. Kosik, Regulation of cell-type-specific transcriptomes by microRNA networks during human brain development. *Nat. Neurosci.* **21**, 1784–1792 (2018). [doi:10.1038/s41593-018-0265-3](doi:10.1038/s41593-018-0265-3) Medline

49. M. Yu, L. Riva, H. Xie, Y. Schindler, T. B. Moran, Y. Cheng, D. Yu, R. Hardison, M. J. Weiss, S. H. Orkin, B. E. Bernstein, E. Fraenkel, A. B. Cantor, Insights into GATA-1-mediated gene activation versus repression via genome-wide chromatin occupancy analysis. *Mol. Cell* **36**, 682–695 (2009). doi:10.1016/j.molcel.2009.11.002 Medline

50. J. A. Gorski, T. Talley, M. Qiu, L. Puelles, J. L. R. Rubenstein, K. R. Jones, Cortical excitatory neurons and glia, but not GABAergic neurons, are produced in the Emx1-expressing lineage. *J. Neurosci.* **22**, 6309–6314 (2002). doi:10.1523/JNEUROSCI.22-15-06309.2002 Medline

51. S. Hippenmeyer, R. L. Johnson, L. Luo, Mosaic analysis with double markers reveals cell-type-specific paternal growth dominance. *Cell Rep.* **3**, 960–967 (2013). doi:10.1016/j.celrep.2013.02.002 Medline

52. D. Jabaudon, M. Scanziani, B. H. Gähwiler, U. Gerber, Acute decrease in net glutamate uptake during energy deprivation. *Proc. Natl. Acad. Sci. U.S.A.* **97**, 5610–5615 (2000). doi:10.1073/pnas.97.10.5610 Medline

53. T. Smith, A. Heger, I. Sudbery, UMI-tools: Modeling sequencing errors in Unique Molecular Identifiers to improve quantification accuracy. *Genome Res.* **27**, 491–499 (2017). doi:10.1101/gr.209601.116 Medline

54. C. H. Teo, S. V. N. Vishwanthan, A. J. Smola, Q. V. Le, Bundle Methods for Regularized Risk Minimization. *J. Mach. Learn. Res.* **11**, 311–365 (2010).

55. P. Shannon, A. Markiel, O. Ozier, N. S. Baliga, J. T. Wang, D. Ramage, N. Amin, B. Schwikowski, T. Ideker, Cytoscape: A software environment for integrated models of biomolecular interaction networks. *Genome Res.* **13**, 2498–2504 (2003). doi:10.1101/gr.1239303 Medline

56. S. Maere, K. Heymans, M. Kuiper, BiNGO: A Cytoscape plugin to assess overrepresentation of gene ontology categories in biological networks. *Bioinformatics* **21**, 3448–3449 (2005). doi:10.1093/bioinformatics/bti551 Medline